Received: 12 April 2019 | Revised: 23 November 2019 | Accepted: 8 December 2019

DOI: 10.1002/ardp.201900108

DPhG ARCH PHARM
Archiv der Pharmazie

FULL PAPER

Pharmacophore modeling, 3D-QSAR, synthesis, and anti-lung cancer evaluation of novel thieno[2,3-*d*][1,2,3]triazines targeting EGFR

Ranza Elrayess[1] | Yasmine M. Abdel Aziz[1] | Mohamed S. Elgawish[2] | Marwa Elewa[1] | Hosam A. Elshihawy[1] | Mohamed M. Said[1]

[1]Department of Pharmaceutical Organic Chemistry, Faculty of Pharmacy, Suez Canal University, Ismailia, Egypt

[2]Department of Medicinal Chemistry, Faculty of Pharmacy, Suez Canal University, Ismailia, Egypt

Correspondence
Mohamed M. Said, Department of Pharmaceutical Organic Chemistry, Faculty of Pharmacy, Suez Canal University, Ismailia 41522, Egypt.
Email: msaid123eg@yahoo.com

Abstract

Two series of thieno[2,3-*d*][1,2,3]triazine derivatives were designed, synthesized, and biologically evaluated as potential epidermal growth factor receptor (EGFR) inhibitors targeting the non-small-cell lung cancer cell line H1299. Most of the synthesized compounds displayed IC_{50} values ranging from 25 to 58 nM against H1299, which are superior to that of gefitinib (40 μM). 3-(5,6,7,8-Tetrahydro-7*H*-cyclohexa[4:5]thieno[2,3-*d*]-1,2,3-triazin-4-ylamino)benzene-1,3-diamine (**6b**) achieved the highest cytotoxic activity against H1299 with an IC_{50} value of 25 nM; it had the ability to decrease the EGFR concentration in H1299 cells from 7.22 to 2.67 pg/ml. In vitro, the IC_{50} value of compound **6b** was 0.33 nM against EGFR, which is superior to that of gefitinib at 1.9 nM and erlotinib at 4 nM. The three-dimensional quantitative structure–activity relationships and molecular modeling studies revealed comparable binding modes of compound **6b**, gefitinib, and erlotinib in the EGFR active site. The in silico ADME (absorption, distribution, metabolism, and excretion) prediction parameters of this compound revealed promising pharmacokinetic and physicochemical properties. Moreover, DFT (density functional theory) calculations showed the high reactivity of compound **6b** toward the EGFR compared with other compounds. The designed compound **6b** might serve as an encouraging lead compound for the discovery of promising anti-lung cancer agents targeting EGFR.

KEYWORDS

3D-QSAR, EGFR, H1299, molecular modeling, thieno[2,3-*d*][1,2,3]triazine

1 | INTRODUCTION

Lung cancer is one of the main causes of death globally due to an ever-increasing percentage of smokers worldwide.[1] Lung cancer represents about one-third of cancer deaths.[2] Non-small-cell lung cancer (NSCLC) is the major type of lung cancer affecting nearly 80–85% of patients.[3,4] Despite the availability of a broad range of chemotherapeutic agents, chemotherapy is still not effective enough in the treatment of patients with advanced NSCLC.[5,6] Therefore, the strategy of drug targeting can bring a solution to this serious problem.[7]

It is worth noting that the epidermal growth factor receptor (EGFR) is overexpressed in NSCLC cell lines of epithelial origin, especially H1299.[8,9] Thus, lowering the EGFR concentration is a plausible target for the design and development of cytotoxic agents targeting H1299 lung cancer cells. EGFR tyrosine kinase inhibitors (EGFR-TKIs) have been extensively used in the

treatment of NSCLC patients.[10] Gefitinib (**I**) and erlotinib (**II**) have been launched by US FDA for the treatment of advanced NSCLC in 2002 and 2004, respectively (Figure 1).[11,12] In spite of the high response rate of NSCLC patients to these agents, the development of drug resistance limits the therapeutic benefits of these two drugs.[13] Therefore, the identification of the second generation of EGFR inhibitors through the discovery of new scaffolds could be beneficial for gefitinib-resisting patients. A rule of thumb, the modulation of the central quinazoline core of the first-generation EGFR inhibitors, gefitinib and erlotinib, could help in improving activity and overcome drug resistance.[14] Various heterocyclic rings have been reported to provide alternatives to the phenyl ring of the central quinazoline core (**III** and **IV**; Figure 1).[15–17] In 2010, cell-based screening protocol has led to the identification of several lead compounds that disturb cell proliferation mediated by abnormal EGFR concentration, among which the tricyclic tetrahydrobenzothieno[2,3-*d*]pyrimidine hit compound (**IV**) has been identified as a prototype with an IC_{50} value of 2.6 μM against EGFR (Figure 1).[15] In 2014, Bugge et al.[18] reported a highly active thienopyrimidine-based EGFR inhibitor (**V**) with an IC_{50} value of 0.3 nM (Figure 1). In 2015, our research group identified novel pyridothieno[3,2-*d*]pyrimidine and alicyclic thieno[1,2,3]triazine scaffolds bearing monocyclic amines as EGFR inhibitors.[17,19] Fortunately, the pyridothieno[3,2-*d*]pyrimidine displayed a promising potency and selectivity toward EGFR with an IC_{50} value of 36 nM (Figure 1).[17]

1.1 | Rationale and design

The success of our research group in designing new classes of tricyclic pyridothieno[3,2-*d*]pyrimidine and thieno[1,2,3]triazine as EGFR inhibitors with promising cytotoxic activities triggered us to develop novel EGFR inhibitors targeting NSCLC.[16,17,19] Moreover, it was found that the majority of the approved and developed first-generation EGFR inhibitors bear the 4-anilino side chains linked to quinazoline/quinoline cores. These side chains occupy an important lipophilic selectivity pocket in the EGFR-binding domain.[20] In light of these facts the pharmacophore modeling, three-dimensional quantitative structure–activity relationship (3D-QSAR), and molecular docking of the two series of tricyclic tetrahydrobenzothieno[2,3-*d*][1,2,3]triazine and dihydrocyclopentathieno-[2,3-*d*][1,2,3]triazine analogs have been used to provide insights into the key structural features required for designing EGFR inhibitors targeting lung carcinoma cell line H1299.[21] The development of this new generation of EGFR inhibitors was based on modulating the 4-anilino side chains with mono- or bicyclic systems and exploring different substituents that could recognize the characteristic lipophilic regions of EGFR. Molecular modeling, 3D-QSAR, in silico

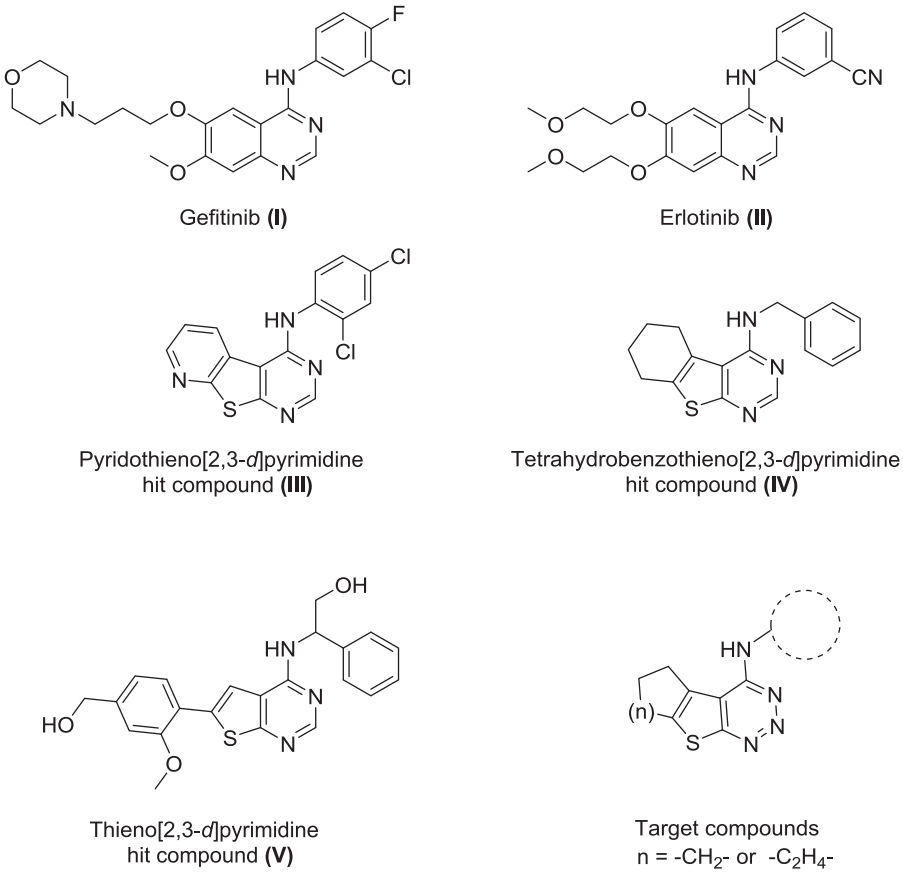

FIGURE 1 Examples of epidermal growth factor receptor inhibitors

ADME (absorption, distribution, metabolism, and excretion) predictions study, Mulliken charge distribution, electrostatic surface potential (ESP), and HUMO/LUMO analysis have been established to confirm our rationale.

2 | RESULTS AND DISCUSSION

2.1 | Chemistry

Cyclopentanone via Gewald reaction afforded 2-amino-5,6-dihydro-4*H*-cyclopenta[*b*]thiophene-3-carbonitrile **2a**. Compound **2a** was diazotized to afford the 4-chlorocyclopenta[4:5]thieno-[2,3-*d*]-1,2,3-triazine **3a**.[19] Compound **3a** was treated with heteroaryl amines, benzylamine, and *m*-phenylenediamine[22] to give different derivatives (**4a**, **4b**, **5a**, **5b**, **6a**, and **7a**). Cyclohexanone underwent Gewald reaction to afford 2-amino-5,6-dihydro-4*H*-cyclohexa[*b*]thiophene-3-carbonitrile **2b**. Diazotization of **2b** afforded the 4-chlorocyclohexa[4:5]thieno-[2,3-*d*]-1,2,3-triazine **3b**.[19] Compound **3b** was allowed to react with heteroaryl amines, benzylamine, and *m*-phenylenediamine.[22] The isoxazolo- and pyrazolo-pyridine derivatives have been prepared from 2-chloro-pyridine-3-carbonitrile derivatives, which underwent the following reaction with hydroxylamine and hydrazine to release the corresponding heteroaryl amines.[16,23]

In general, the infrared (IR) spectra displayed a secondary amine peak at 3,300–3,500 cm^{-1}, which indicated the coupling of compounds **3a** and **3b** with different amines and peak for (C–S) at the range of 690–830 cm^{-1}. ^{1}H-NMR (nuclear magnetic resonance) spectra of the new compounds showed the appearance of multiplet peaks of aromatic protons at the range of 6–8 δ (ppm) and the characteristic upfield signals corresponding to aliphatic protons of both cyclohexanone and cyclopentanone at the range of 1–3 δ (ppm). In addition, the ^{1}H-NMR spectra of compounds **4b**, **4d**, **5b**, and **5d** showed two sharp peaks corresponding to the two methyl groups of the isoxazolo- and pyrazolo-pyridine moiety at the range of 2.52–3.65 δ (ppm). The ^{1}H-NMR spectra of compounds **7a** and **7b** showed the characteristic singlet peak for CH_2 of the benzylamine moiety at 3.86 and 4.24, respectively.

2.2 | Biology

2.2.1 | Cytotoxic activity against H1299

The potential anticancer activity of the new compounds was evaluated using sulforhodamine-B assay against NSCLC cell line H1299.[24] It is well-known that EGFR is overexpressed in (H1299).[25] It was observed that all the newly synthesized compounds displayed remarkable inhibitory activities against the lung carcinoma cell line (H1299) with IC_{50} values ranging from 25 to 48 nM superior to that of gefitinib 40 μM. The results are summarized in Table 1.

TABLE 1 In vitro cytotoxic activity of the synthesized compounds against the NSCLC (non-small-cell lung cancer) cell line H1299

Compound	IC_{50} against H1299
4a	31 nM
4b	56 nM
5a	37 nM
5b	56 nM
7a	42 nM
4c	28 nM
4d	53 nM
5c	34 nM
5d	30 nM
6b	25 nM
7b	30 nM
Gefitinib	40 μM

2.2.2 | Measurement of human EGFR in H1299 cell culture

Compound **6b** had the ability to decrease EGFR concentration in the H1299 cell line from 7.22 to 2.67 pg/ml. On the contrary, gefitinib decreased EGFR concentration to 3.72 pg/ml. This indicates that compound **6b** inhibits the growth of NSCLC cell line H1299 through EGFR inhibition. The results are summarized in Table 2.

2.2.3 | Measurement of potential EGFR inhibitory activity IC_{50}

Compound **6b** displayed an IC_{50} value of 0.33 nM, which is superior to those exerted by the reported thienopyrimidine derivative 36 nM,[17] gefitinib 1.9 nM, and erlotinib 4 nM.

2.3 | Pharmacophore and 3D-QSAR models

In this study, the pharmacophore generation model was developed using the pharmacophore modeling task of Schrodinger (10.1). Twelve synthesized compounds are considered with promising activity against the H1299 cancer cell line in the 3D-QSAR pharmacophore model. Phase supplies a built-in set of six pharmacophore features: hydrogen bond acceptor (A), hydrogen bond donor

TABLE 2 Measurement of epidermal growth factor receptor (EGFR) concentration in the lung cancer cell line H1299

Compound	IC_{50} against H1299	EGFR concentration (pg/ml) in H1299
No compound	–	7.22
6b	25 nM	2.67
Gefitinib	40 μM	3.72

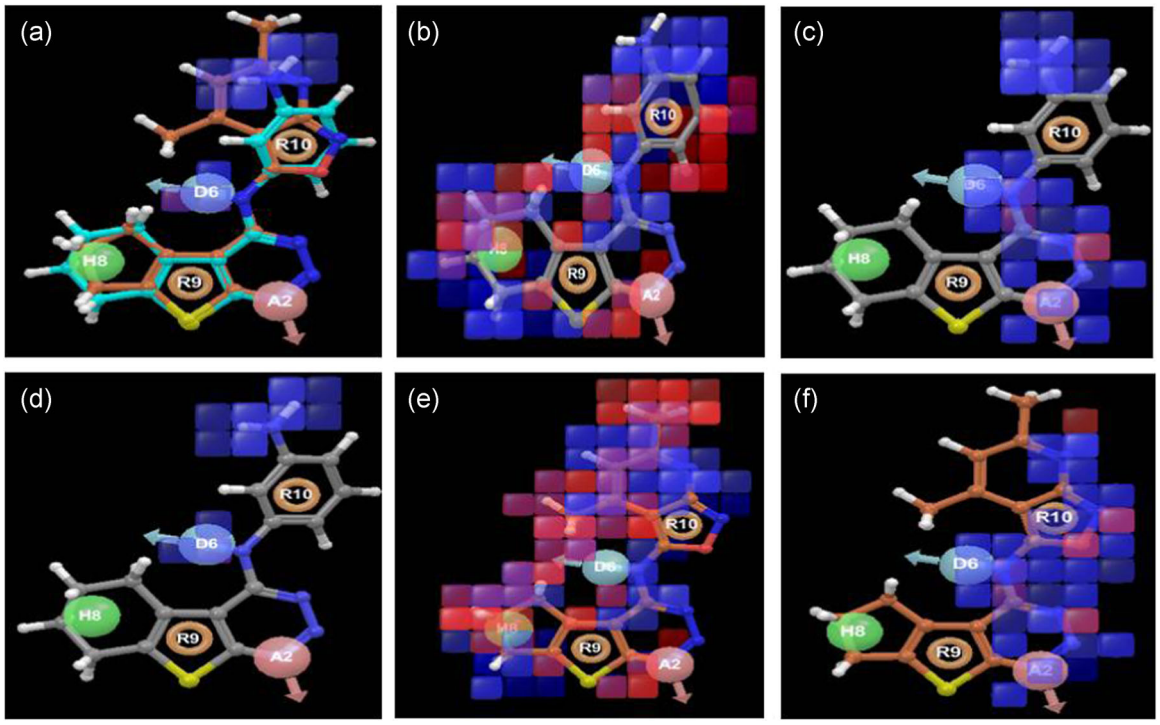

FIGURE 2 Quantitative structure–activity relationship model visualized in the context of favorable and unfavorable hydrogen bond donor effects in (a, d), hydrophobic interactions in (b, e), and electron-withdrawing groups in (c, f) for the highest and lowest active compounds **6b** and **4a**, respectively

(D), hydrophobic group (H), negatively charged group (N), positively charged group (P), and aromatic ring (R). Atom-based 3D-QSAR revealed how substitution can influence biological activity. Twelve common pharmacophore models were generated with a different combination of variants (AAADH, AAADR, AAAHR, AAARR, AADHR, AADRR, AAHRR, AARRR, ADHRR, ADRRR, AHRRR, and DHRRR). Among these pharmacophore models, ADHRR showed the best survival score and an optimum alignment with active compounds. Thus, it was selected to generate the QSAR model. Ten predictive pharmacophore models of the variant AAHHR were generated (Table 1 and Supporting Information). All the generated pharmacophore models kept at least five chemical features. The models with maximum adjusted survival scores were chosen for creating the atom-based alignment of EGFR inhibitors. Model ADHRR.26 has been carefully chosen because it generated good alignment of active ligands in comparison with inactive ones. The special arrangement of features along with their distances present in five-featured pharmacophore ADHRR is shown in Figure 1 and the Supporting Information. As depicted in Figure 2a–f, the hydrogen bond acceptors in 12 training are mapped to *N*-triazine. The hydrogen bond donors are mapped to NH-amino group. The hydrophobic groups are mapped to cyclopentyl or cyclohexyl, whereas aromatic ring features are mapped to thiophene, phenyl, pyrazole, or isoxazole moieties as shown in Figure 2a–f.

The six compounds (test set) also showed the same feature map of the training set. Moreover, gefitinib and two of the reported ligands with potent inhibition against EGFR exhibited more or less the same feature map (Figure 3 and Supporting Information). In gefitinib, the hydrogen bond acceptor is mapped to *N*-pyrimidine. The hydrogen bond donors are mapped to the NH-amino group at C4 of quinazoline. The hydrophobic groups are mapped to the methoxy group, whereas the aromatic ring features are mapped to a benzoid group of quinazoline and phenyl group adjacent to the NH group. The 3D-QSAR model was created using the partial least squares (PLS) regression statistics. The grid spacing was kept at 1 Å. The number of PLS factors included in the model development is 3 (Table 3). The best-fitted model ADHRR.26 ($R^2 = 0.9908$, $Q^2 = 0.8493$, and $F = 97.10$) consists of one hydrophobic interaction, one hydrogen

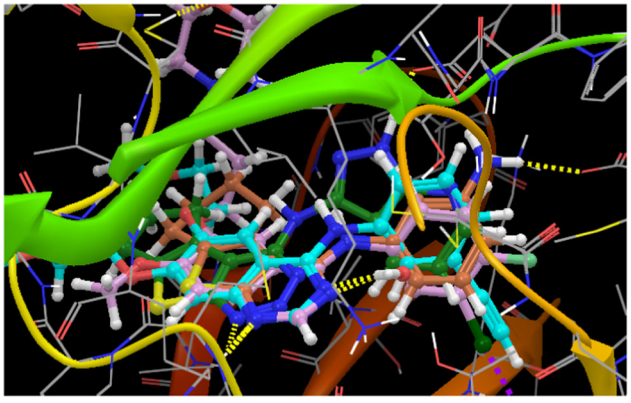

FIGURE 3 Three-dimensional-binding modes and overlay of erlotinib, gefitinib, compounds **6b** and **4a** in the catalytic domain of epidermal growth factor receptor (PDB 1M17)

TABLE 3 PLS statistical parameters of the model ADHRR.26

PLS	*SD*	R^2	*F*	*p* value	Stability	RMSE	Q^2	Pearson's *R*
1	0.1259	0.8682	85.6	4.394e−007	−0.5372	0.1267	0.0938	0.310
2	0.0722	0.9599	143.7	4.139e−009	−0.5763	0.0842	0.2365	0.5342
3	0.0362	0.9908	393.9	1.801e−011	−0.6285	0.1008	0.7287	0.4283

Abbreviations: PLS, partial least squares; RMSE, root mean square error; *SD*, standard deviation.

bond donor, one hydrogen bond acceptor, and two aromatic features. The distance and angles between different sites of the model ADHRR.26 are presented in Table 3 and Supporting Information.

2.3.1 | 3D-QSAR contour map analysis

The 3D-QSAR models with combined effects of electron-withdrawing, hydrogen bond donor, as well as hydrophobic/nonpolar are displayed in Figure 2a–f. The blue regions indicated favorable interactions between ligand and target enzymes. On the contrary, the red regions indicated unfavorable features. The effect of the hydrogen bond donor is presented by the blue cube on the amino group on C4 of the triazine ring of the highest active and nearly all synthesized compounds. The majority of the approved drugs bear this amino group. Thus, the presence of the amino group is essential for the EGFR inhibitory activity. Moreover, the presence of another blue cube near to the amino group at the meta position of the 4-anilino group gives the compounds **6a,b** with this electron-donating amino group the biological superiority. Compound **6b** with the *m*-amino group had shown more cytotoxic activity than its analog compound **7b**, which lacks this important group. The hydrophobic contour of the highest active compounds revealed the necessity of hydrophobic interaction of 4-anilino group and other bicyclic systems. In addition, *para* substitution of 4-anilino group gave extra hydrophobic interaction and this is consistent with the high potency of gefitinib. Another important position for hydrophobic interaction was the cyclohexenyl group adjacent to thiophene; modifying cyclohexyl to cyclopentenyl could influence the biological activity as shown in compound **6a** compared with compound **6b**. We attributed this observation to the occupation of cyclopentenyl ring near to red cube (Figure 2a–f). The lowest cytotoxic compound (**5b**) in our series unveiled that the two methyl substitutions on isoxazolopyridine are occupied in the red region and thus, unfavored for the activity. The electron-withdrawing contour is obviously shown at the *meta* and *para* positions of anilino attached to triazine. The blue cube at the aforementioned positions revealed the necessity of electron-withdrawing at this position. This is clear in the approved EGFR inhibitors gefitinib and erlotinib, which contain chloro and cyano groups, respectively.

2.3.2 | Pharmacophore model validation

The selection of the generated pharmacophore model (ADHRR26) was on the basis of its validation. A 3D-QSAR study was carried on the six synthesized compounds (test set) to explore the reflection of the spatial arrangement of structural features on the EGFR inhibition (Table 3). The stability of a statistically significant regression model is specified by the high value of *F* (393.9) and a high degree of confidence along with the small value of variance ratio *p* (1.801e −011). In addition, the data used for model generation are optimum for the QSAR analysis. This is understandable from the small values of RMSE (0.1008) and standard deviation (0.0326) and from the high value of R^2 (squared correlation coefficient value; 0.9908). The model was validated by the cross-validated correlation coefficient, Q^2 (0.7287), which was obtained by the leave-one-out or leave-*N*-out method (Table 3). The statistical parameter of Q^2 is more reliable than that of R^2. The scatter plots for experimental and predicted activities of synthesized molecules indicated a significant linear correlation as shown in Figure 3a,b and Supporting Information. Validation for the generated pharmacophore model (ADHRR26) was done by mapping one approved drug gefitinib and two reported compounds, tetrahydrobenzothieno[3,2-d]pyrimidine,[26] with EGFR inhibitory activity. Their fit values and the fit values of the tested compounds and their predicted and experimental activity were compared using our ligand pharmacophore mapping protocol (Table 4). The expected activities of these compounds and the training set through the pharmacophore model as well as their fit values are presented in Table 4. It is worth noting that the expected cytotoxic activity created by the 3D pharmacophore QSAR model was closely related to that of experimentally observed. Therefore, these QSAR models could be safely applied for predicting the cytotoxicity of new compounds.

2.4 | Molecular docking

In this study, the activity of tetrahydrobenzothieno[2,3-*d*][1,2,3]-triazine and dihydrocyclopentathieno[2,3-*d*][1,2,3]triazine derivatives toward EGFR was explained using Glide docking of the Schrodinger program. The synthesized compounds were docked well in the erlotinib-binding site and set up many electrostatic interactions as well as hydrogen bonding and hydrophobic interactions (Figure 3). LEU 694, LEU 768, PHE 771, PRO 770, GLY 772, MET 769, and CYS 773 were the main amino acids involved in these interactions. Generally, tetrahydrobenzothieno[2,3-*d*][1,2,3]triazine scaffold, especially tetrahydrobenzene and thiophene moieties, exhibited hydrophobic interaction with LEU 694, PRO 770, and CYS 773.

This scaffold occupied a deep pocket at the back of the adenosine triphosphate (ATP)-binding site (Figure 3). In addition, phenyl, isoxazole-pyridine, and pyrazolo-pyridine attached to triazine via

TABLE 4 Calculated pIC_{50} for designed, approved, and reported compounds

In	Ligand name	QSAR set	Activity	Predicted activity	Pharm set	Residual activity	Fitness
1	**4a**	Test	7.50	7.41	Active	0.09	3.00
2	**4b**	Training	7.25	7.24	Active	0.01	2.84
3	**5a**	Training	7.43	7.42	Active	0.01	2.95
4	**5b**	Test	7.23	7.28	Active	−0.05	2.82
5	**6a**	Training	7.53	7.54	Active	−0.01	2.62
6	**7a**	Test	7.37	7.35	Active	0.02	2.07
7	**4c**	Training	7.55	7.47	Active	0.08	2.48
8	**4d**	Training	7.27	7.33	Active	−0.06	2.73
9	**5c**	Training	7.46	7.47	Active	−0.01	2.48
10	**5d**	Test	7.52	7.43	Active	0.07	2.71
11	**6b**	Training	7.60	7.64	Active	−0.04	2.56
12	**7b**	Training	7.52	7.51	Active	0.01	2.07
13	Gefitinib		7.76	7.74	Active	0.02	1.46
14	DER-3		6.48	6.48	Active	0.00	1.62
15	DER-4		6.76	6.75	Active	0.01	2.17

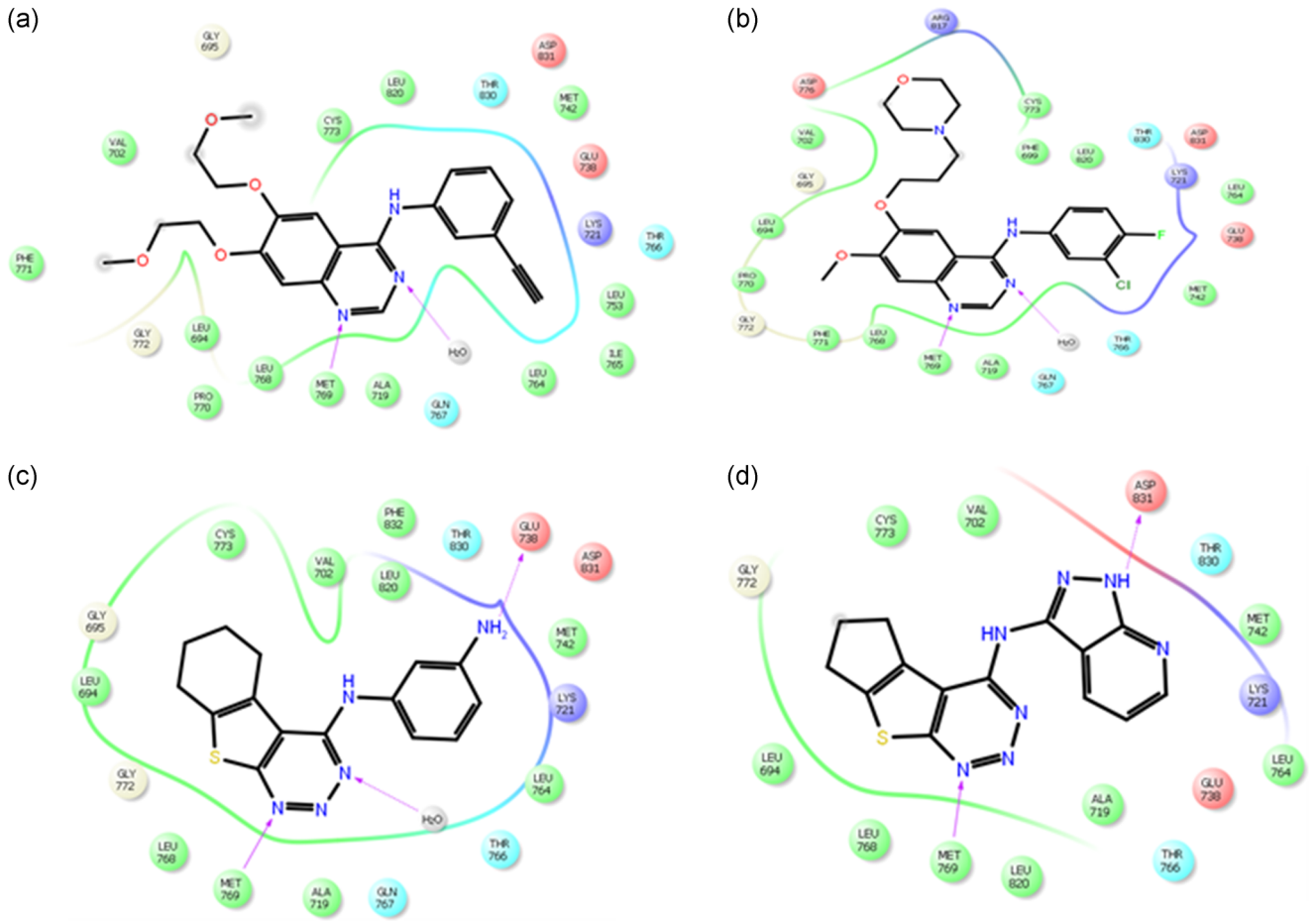

FIGURE 4 Two-dimensional ligand–receptor interactions of (a) erlotinib, (b) gefitinib, (c) compound **6b**, and (d) compound **4a** in the catalytic domain of the epidermal growth factor receptor (1M17)

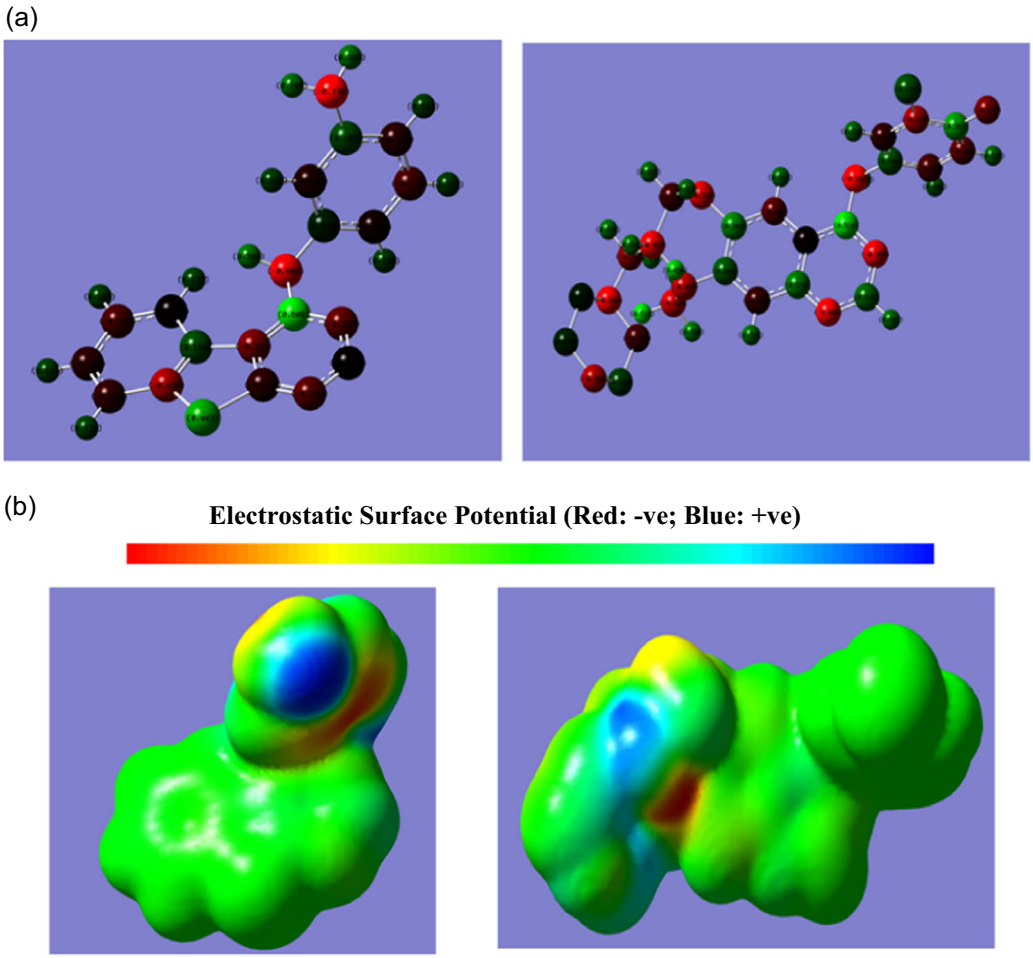

FIGURE 5 (a) Mulliken charges, (b) electrostatic surface potential calculated using 6–311++G (d,p) basic set methodology (color-coded from red to blue) and density functional theory method with B3LYP functional

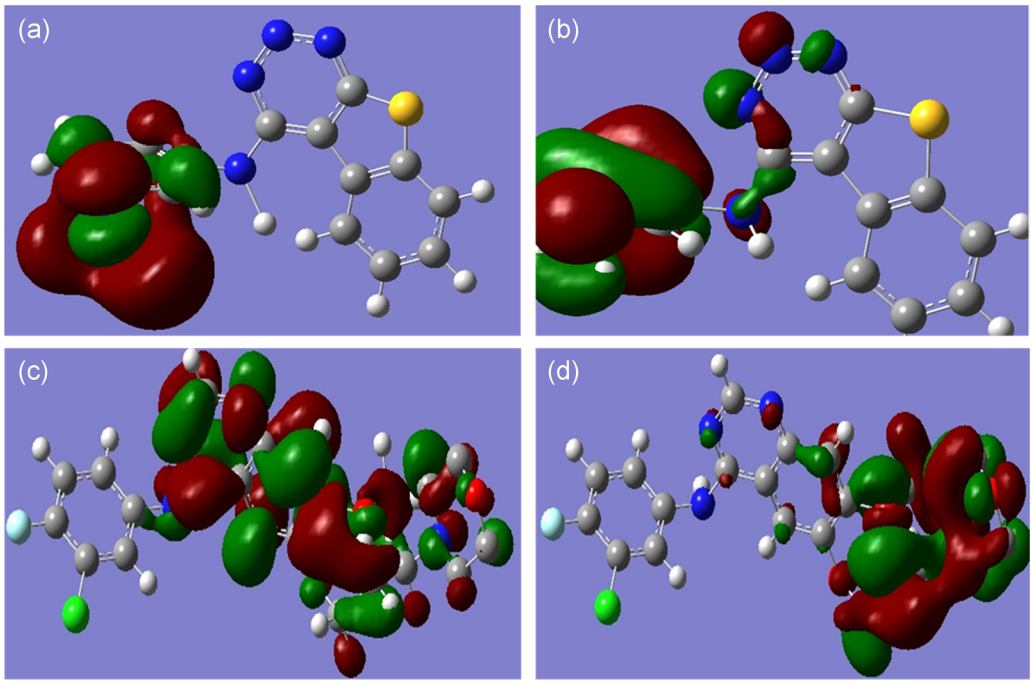

FIGURE 6 Plots of HOMO and LUMO of compound **6b** (a, b) and gefitinib (c, d)

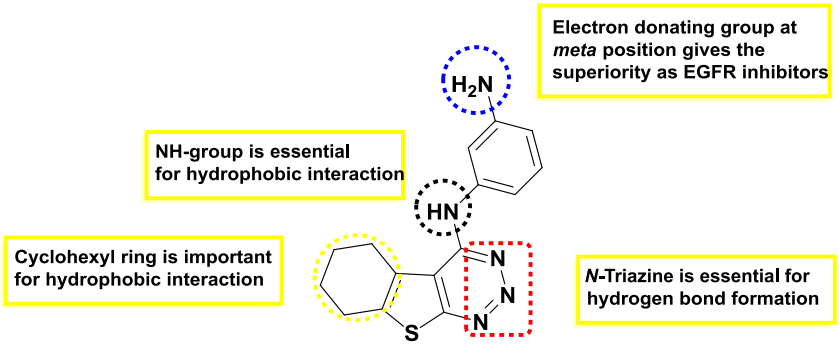

FIGURE 7 The observed structure–activity relationships of the newly synthesized compounds against H1299. EGFR, epidermal growth factor receptor

NH linkage also revealed hydrophobic interaction with CYS 751, PHE 832, TYR 703, LEU 764, LEU 753, MET 742, and ILE 720. As evident, both the above scaffolds are buried within the hydrophobic pocket, which could give our compound stabilization at an active site. The *m*-amino group on the phenyl group and NH of pyrazole also showed polar interaction with ALA 698 and THR 766 residues. This polar interaction gave pyrazole derivative a superior affinity compared with isoxazole, which lacks this hydrophilic interaction. The docked structure of compound **6b** indicated that this compound fits reasonably in the receptor cavity (Figure 3). N-1 of triazine interacted via a hydrogen bonding of 2.08 Å with MET 769, and N-3 made water-mediated H-bond of 2.07 Å to the side chain of THR 766.

Moreover, NH_2 at *meta* position of aniline and NH of pyrazole interacted via hydrogen bond of 2.09 Å and 1.6 Å with GLU 738 and ASP 831. These extra hydrogen bonding could give our compound the high affinity and stability within the active receptor site compared with erlotinib, the EGFR TK inhibitor cocrystallized within the receptor site (PDB 1M17). Our docking results came in consistency with the result of 3D-QSAR pharmacophore modeling. Compared with the approved EGFR TK inhibitors, our compounds showed optimum hydrophilic, hydrophobic, and hydrogen bond interactions as shown in Figure 4a–d.

The accuracy of our docking procedure was confirmed by checking the interaction of the erlotinib to 1M17 receptor after grid generation. Glide docking of erlotinib showed the same pose and interaction with the receptor as that in grid generation. In addition, the accuracy could be checked by examining the docking score and Glide emodel. Compound **6b** had the highest docking score of −7.128 and Glide emodel of −65.055, whereas compound **5b** showed −5.76 and −54.54 of docking score and Glide emodel. These results came close to the potency of these compounds as EGFR inhibitor. Gefitinib and erlotinib showed −6.32 and −6.79 of docking score and −86.11 and −86.68 of Glide emodel, respectively.

2.5 | Computational study

The energy calculation in Gaussian 09 software using the density functional theory (DFT) method on the crystallized conformation of gefitinib and the most active compound **6b** was run to visualize the charge distribution on both compounds, to better understand the chemical reactivity of molecules, and to estimate the contribution of polar and nonpolar interactions in their binding to EGFR. The Mulliken charge distribution for all the atoms as well as the ESP for gefitinib and compound **6b** were calculated using the B3LYP functional with a 6–311++G (d,p) basis set. In Figure 5a, the calculated atomic charge of the nitrogen atom of triazine in compound **6b** and pyrimidine in gefitinib interacting with MET 769 and THR 766 in hinge region was found to be (−0.23 to −0.608). This fortified the hydrogen bond (HBA) formation and highlighted the significance of interaction for EGFR selectivity. Interestingly, the high negative atomic charge of aniline NH of −0.77 expected hydrogen bond or salt bridge formation with GLU 738 in gatekeeper residue. Shape and size difference is apparently observed in the ESP of both compounds (Figure 5) with mostly two arms of gefitinib. The noticeable difference is the strong positive charge localized on the right arm of *m*-amino aniline of compound **6b** that gives it the superiority to tightly bind within gatekeeper residue. This, to some extent, explained the novelty of the designed compound toward EGFR. The inclusion of the electron-donating group, NH_2, instead of Cl, F, and CN in most of EGFR inhibitors represent a new discovery in PTK inhibition. The molecular docking study came in agreement with computational study, where nitrogen of triazine ring besides *m*-amino group of aniline are involved in important interaction with the key residue of the hinge region, gatekeeper, and hydrophobic pocket.

The orbital energies of HOMO and LUMO of most active compound **6b** were calculated using Gaussian 09 software. The HOMO and LUMO sites were plotted on the molecular surface of compound **6b** as shown in Figure 6. The analysis of HOMO maps of compound **6b** showed that HOMO molecular orbitals are located on *m*-amino aniline and three nitrogen atoms of triazine moiety, indicating their involvement in protein–ligand interaction. On the contrary, the LUMO molecular orbitals are located on *m*-amino phenyl moiety of compound **6b**. Docking study revealed the involvement of these moieties in hydrogen bond formation with key residues of the hinge region and gatekeeper residue and hydrophobic. Figure 7 summarizes the cytotoxic activity against H1299 depending on the observed structure–activity relationships.

2.6 | Lipinski's rule for drug likeliness and in silico ADME prediction

Pharmacokinetic features for the most active compound (**6b**) were calculated utilizing ADME predictions by QikProp v4.3 function of

TABLE 5 In silico ADME prediction parameters of the designed and reference molecules

Compound	mol_MW[a]	donorHB[b]	accptHB[c]	QPlogP o/w[d]	No. of rotors[e]	PSA[f]	QPlogS[g]	QPlogHERG[h]	QPPCaco[i]	QPPMDCK[j]	QPlogKhsa[k]	Human oral absorption (%)[l]
6b	279.37	2.5	5	2.35	3	76.56	−4.08	−5.22	468.67	388.59	0.05	88.56
Gefitinib	446.90	1	7.7	4.01	8	66.03	−5.22	−6.54	626.02	1,306.11	0.31	100.00

Note: Acceptable ranges: [a]<500 amu; [b]<5; [c]<10; [d]<5; [e]0–15; [f]7–200; [g]<0.5; [h]≤5; [i]<25 poor, >500 great; [j]<25 poor, >500 great; [k]−1.5 to 1.5; [l]>80% is high, <25% is poor.
Abbreviations: ADME, absorption, distribution, metabolism, and excretion; HB, hydrogen bond; hsa, human serum albumin; o/w, octanol/water.

Schrodinger 10-1 (Table 4). The compound **6b** was estimated for its fundamental parameters of Lipinski's rule of five. The oral bioavailability of the drug molecules could be controlled by polar surface area (7–200 Å) and the value of rotatable bonds (0–15). Caco-2 cell permeability (QPPCaco) was used as a model for the gut–blood barrier by nonactive transport. This is a marker for intestinal absorption or permeation. Caco-2 cell permeability of the test compound **6b** showed good results predicting excellent drug permeability compared with gefitinib. The cell permeability of the blood–brain barrier (BBB) was expected by QPPMDCK descriptor. MDCK cells are a good mimic for BBB. Compound **6b** exhibited good BBB permeability (QPPMDCK > 25). Another important descriptor is QPlogkhsa descriptor of QikProp that predicts human serum albumin-binding capability. Compound **6b** showed reasonable binding to plasma proteins. QPlogP o/w and QPlogS are descriptors of octanol/water partition coefficient and aqueous solubility; the test compound was found to be in the permissible range (Table 4). The most active compound **6b** was considered as a promising lead molecule for designing potent EGFR inhibitors with excellent membrane permeability and oral bioavailability. The physicochemical properties of other designed compounds were enough to permeate our drug through GIT. Compounds **4a–d** and compounds **5a–d** having bicyclic system-substituted pyrazolo-pyridine and isoxazole-pyridine showed the highest partition coefficient and consequently highest penetration disclosed by great value of QPPCaco and human oral absorption % (data not shown). In silico ADME prediction results came in agreement with the in vitro study; compound **6b** achieved the superior cytotoxic activity against H1299. Alternatively, gefitinib showed excellent in silico ADME result including good partition coefficient, permeability, and oral bioavailability (Table 5).

Moreover, most of the kinase inhibitors bind to the ATP-binding site of the enzyme in its active "DFG-in" state. Such molecules are known as type I inhibitors that mimic the interaction of the adenine ring of ATP with the hinge region.[27] Type I EGFR inhibitors involve the approved marketed drugs gefitinib and erlotinib. Selective inhibitors create interactions with the hydrophobic back cavity of the ATP-binding site. Type I inhibitors can achieve certain level of selectivity when the substituted phenyl ring attached to C4 of quinazoline via NH occupies the selectivity pocket. In the design of our compounds, we kept this ring in certain series and modified it to pyrazolo-pyridine and isoxazole-pyridine in another series in an attempt to study how this variation could affect the biological activity and binding mode. We found that the phenyl ring was the optimum considering molecular docking and biological activity. Type I EGFR inhibitors have the electron-withdrawing moiety attached to the phenyl ring, like Cl in case of gefitinib and CN in case of erlotinib. Meanwhile, in this study, another strategy was applied; electron-withdrawing moiety was changed with electron-donating group. *Meta* position of phenyl ring was substituted with NH_2, which gave our compound the chance to form hydrogen bond with GLU 738 and one DFG motif, ASP381 and this was clearly observed by the high negative atomic charge of NH (−0.77) in Mulliken charge distribution. This additional interaction could enhance the EGFR inhibitory activity and drug affinity to EGFR. Compound **6b** achieved the highest potency, affinity, and stability as shown by its lowest IC_{50} 0.33 nM, highest docking

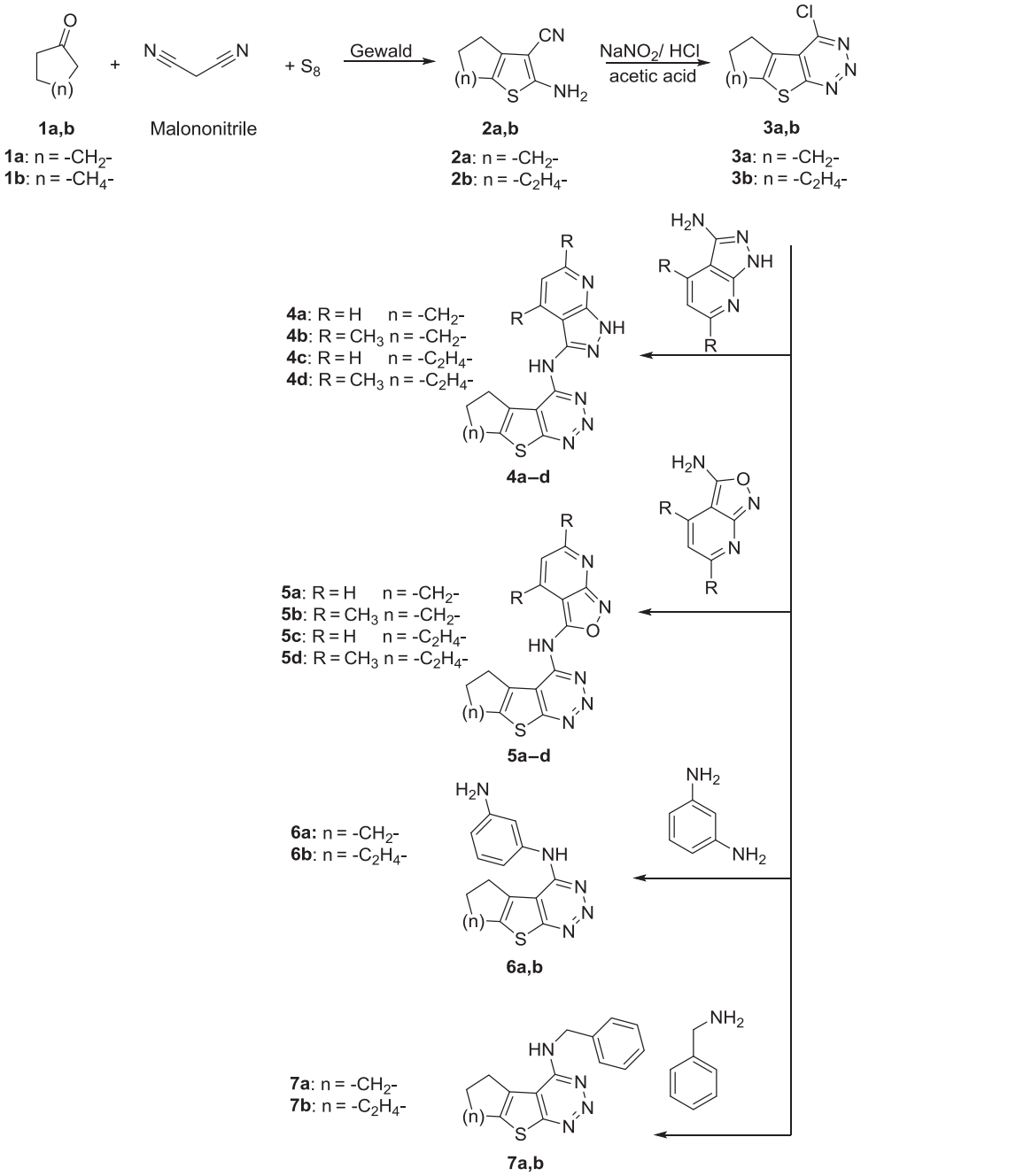

SCHEME 1 Synthesis of dihydrocyclopentathieno and tetrahydrobenzothieno triazine derivatives

score and lowest Glide model energy. Increasing one atom between NH appended at C4 of triazine and phenyl group could influence the affinity and biological activity and this was obviously seen in compounds **7a,b** compared with compounds **6a,b**.

3 | CONCLUSION

The novel synthesized compounds exhibited highly potent cytotoxic activity toward NSCLC cell line H1299 with IC_{50} values ranging from 25 to 58 nM, superior to that of gefitinib 40 μM. The antiproliferative activity of the designed compounds was expected to be through EGFR inhibition. Fortunately, the most active compound **6b** decreased EGFR concentration in the H1299 cell line from 7.22 to 2.67 pg/ml. The molecular modeling study explained the potent inhibitory activity of the most active compound **6b**. Moreover, compound **6b** showed an IC_{50} value of 0.33 nM against EGFR superior to that of gefitinib 1.9 nM and erlotinib 4 nM. Tetrahydrobenzothieno[2,3-*d*][1,2,3]triazine scaffold occupied the ATP-binding site showing the same drug–receptor interaction like the approved drugs gefitinib and erlotinib. Additional bindings were provided by our structural modification. The atom-based 3D-QSAR generated a model ADHRR that exhibited good correlation (R^2), cross-validation (Q^2) coefficients, and excellent agreement between

experimental and predictive activities. Molecular orbital (HOMO/LUMO) analysis, ESP, and Mulliken charge distribution were beneficiary tools in understanding the chemical reactivity of designed molecules with EGFR. Our new thienotriazine scaffold might serve in the development of EGFR inhibitors targeting NSCLC cell line H1299.

4 | EXPERIMENTAL

4.1 | Chemistry

4.1.1 | General

The commercial chemicals and solvents for the synthesis were reagent grade and used without further purification. Varian Mercury VX-300 NMR spectrometer or Jeol LA (400 MHz for ^{1}H-NMR, 100 MHz for ^{13}C-NMR) were used to measure ^{1}H- and ^{13}C-NMR spectra. Electron impact mass spectra (EI-MS) were recorded on Shimadzu GCMS-QP 5050 A gas chromatograph-mass spectrometer (70 eV). Melting points (m.p.) were determined in open capillaries using Gallenkamp melting point apparatus and are uncorrected. Infrared (IR) spectra were recorded on a Shimadzu FT-IR 8101 PC IR spectrophotometer (KBr pellets). The synthetic procedures for the target compounds are illustrated in Scheme 1.

The InChI codes of the investigated compounds together with some biological activity data are provided as Supporting Information.

*2-Amino-5,6-dihydro-4H-cyclopenta[b]thiophene-3-carbonitrile (**2a**)*
Sulfur (127 mg, 3.96 mmol) was added to a solution of cyclopentanone (3.96 mmol) in ethanol (25 ml) and malononitrile (3.96 mmol). The mixture was stirred at 45°C. Morpholine (5.54 mmol) was added dropwise over 15 min. The mixture was further stirred at 60°C for 18 hr. The mixture was filtered while hot and the resulting crystals were washed with 30% ethanol and dried.[28] Melting point: 135–137°C (yield: 80%), as reported.[28] Mass spectrum: *m/z* (%): 166 (M^{+}+2), 164, 137, 121, 68, and 43.

*4-Chlorocyclopenta[4:5]thieno[2,3-d]-1,2,3-triazine (**3a**)*
A solution of sodium nitrite (1 gm, 16 mmol) was added to a mixture of compound **2a** (10 mmol), HCl (10 ml, 5%) and glacial acetic acid (10 ml). The mixture was stirred at 0–5°C for 1 hr, then for 2 hrs at 20°C. The mixture was poured into 100 ml of water and the precipitate was separated by filtration, washed with water, and dried.[19] Melting point: 200°C (yield: 81.8%), as reported. Mass spectrum: *m/z* (%): 213 (M^{+}+2), 212, 211, 199, 196, and 172.

4.1.2 | General procedure for the synthesis of compounds 4a,b, 5a,b, 6a, and 7a

A mixture of equimolar amounts (0.01 mol) of compound **3a** and the aromatic amines in dry pyridine (10 ml) was refluxed for 16 hr. The mixture was filtered while hot and washed with ice-water. The precipitate was then recrystallized from ethanol.[22]

*N-(5,6-Dihydro-7H-cyclopenta[4:5]thieno[2,3-d]-1,2,3-triazin-4-ylamino)pyrazolo[3,4-b]pyridin-3-amine (**4a**)*
Melting point: >300°C (yield: 60%). Mass spectrum: *m/z* (%): 309 (M^{+}), 307, 291, 208, 119, and 75. IR (cm^{-1}): 771 (C–S), 1,288 (C–N), 1,624 (C=N), and 3,421 (N–H), ^{1}H-NMR (dimethyl sulfoxide [DMSO]-d_6, 400 MHz): δ (ppm) = 1.34–1.17 (m, 2H, H-2), 1.93 (t, J = 7.1 Hz, 2H, H-1), 2.73 (t, J = 7.1 Hz, 2H, H-3), 3.60 (s, 1H, H-4), 7.35–7.19 (m, 3H, Ar–H), and 9.69 (s, 1H, H-5). Elemental analysis calculated for $C_{14}H_{11}N_7S$: C, 54.36; H, 3.58; N, 31.69. Found: C, 54.61; H, 3.64; N, 31.98.

*N-(5,6-Dihydro-7H-cyclopenta[4:5]thieno[2,3-d]-1,2,3-triazin-4-ylamino)4,6-dimethylpyrazolo[3,4-b]pyridin-3-amine (**4b**)*
Melting point: >300°C (yield: 65%). Mass spectrum: *m/z* (%): 337 (M^{+}), 313, 287, 199, 148, and 146. IR (cm^{-1}): 713 (C–S), 1,334 (C–N), 1,654 (C=N), 3,356 (N–H), and 3,421 (N–H). ^{1}H-NMR (DMSO-d_6, 400 MHz): δ (ppm) = 1.91–1.76 (m, 2H, H-2), 2.41 (t, J = 7.1 Hz, 2H, H-1), 2.49 (t, 2H, J = 7.1 Hz, H-3), 2.52 (s, 3H, CH_3), 2.54 (s, 3H, CH_3), 5.10 (s, 1H, H-4), 6.58 (s, 1H, Ar–H), and 11.78 (s, 1H, H-5). Elemental analysis calculated for $C_{16}H_{15}N_7S$: C, 56.96; H, 4.48; N, 29.06. Found: C, 57.21; H, 4.53; N, 29.24.

*N-(5,6-Dihydro-7H-cyclopenta[4:5]thieno[2,3-d]-1,2,3-triazin-4-ylamino)oxazolo[3,4-b]pyridin-3-amine (**5a**)*
Melting point: >300°C (yield: 62%). Mass spectrum: *m/z* (%): 310 (M^{+}), 299, 284, 216, 146, and 42. IR (cm^{-1}): 752 (C–S), 1,273 (C–O), 1,624 (C=N), and 3,417 (N–H). ^{1}H-NMR (DMSO-d_6, 400 MHz): δ (ppm) = 1.42–1.22 (m, 2H, H-2), 2.58 (t, J = 7.1 Hz, 2H, H-1), 2.71 (t, J = 7.1 Hz, 2H, H-3), 3.34 (s, 1H, NH), and 7.12–6.98 (m, 3H, Ar–H). Elemental analysis calculated for $C_{14}H_{10}N_6OS$: C, 54.18; H, 3.25; N, 27.08. Found: C, 54.37; H, 3.21; N, 27.41.

*N-(5,6-Dihydro-7H-cyclopenta[4:5]thieno[2,3-d]-1,2,3-triazin-4-ylamino)-4,6-dimethyloxazolo[3,4-b]pyridin-3-amine (**5b**)*
Melting point: >300°C (yield: 64%). Mass spectrum: *m/z* (%): 338 (M^{+}), 330, 298, 239, 222, and 99. IR (cm^{-1}): 740 (C–S), 1,157 (C–O), 1,273 (C–N), 1,627 (C=N), and 3,421 (N–H). ^{1}H-NMR (DMSO-d_6, 400 MHz): δ (ppm) = 1.82–1.65 (m, 2H, H-2), 2.49 (t, J = 7.1 Hz, 2H, H-1), 2.55 (s, 3H, CH_3), 2.59 (s, 3H, CH_3), 2.71 (t, J = 7.1 Hz, 2H, H-3), 7.31 (s, 1H, Ar–H), and 10.83 (s, 1H, NH). Elemental analysis calculated for $C_{16}H_{14}N_6OS$: C, 56.79; H, 4.17; N, 24.84. Found: C, 57.01; H, 4.20; N, 24.72.

*3-(5,6-Dihydro-7H-cyclopenta[4:5]thieno[2,3-d]-1,2,3-triazin-4-ylamino)benzene-1,3-diamine (**6a**)*
Melting point: >300°C (yield: 40%). Mass spectrum: *m/z* (%): 285 (M^{+}+2), 284, 283, 266, 246, and 44. IR (cm^{-1}): 790 (C–S), 1,620 (C=N), 3,221 (N–H), and 3,348 (NH_2). ^{1}H-NMR (DMSO-d_6, 400 MHz): δ (ppm) = 1.41–1.23 (m, 2H, H-2), 2.33 (t, J = 7.1 Hz, 2H, H-1), 2.67 (t, J = 7.1 Hz, 2H, H-3), 4.39 (s, 1H, NH)), 8.21–7.85 (m, 3H, Ar–H), 7.91

(s, 1H, ArH-4), and 10.15 (s, 2H, NH_2). Elemental analysis calculated for $C_{14}H_{13}N_5S$: C, 59.34; H, 4.62; N, 24.72. Found: C, 59.67; H, 4.71; N, 25.03.

*3-(5,6-Dihydro-7H-cyclopenta[4:5]thieno[2,3-d]-1,2,3-triazin-4-ylamino)benzylamine (**7a**)*

Melting point: 224–226°C (yield: 70%). Mass spectrum: *m/z* (%): 284, (M^++2), 283, 282, 269, 250, and 91. IR (cm^{-1}): 752 (C–S), 1,350 (C–N), 1,597 (C=N), and 3,336 (N–H). ^{1}H-NMR (DMSO-d_6, 400 MHz): δ (ppm) = 1.42–1.23 (m, 2H, H-2), 1.81 (t, J = 7.1 Hz, 2H, H-1), 2.72 (t, J = 7.1 Hz, 2H, H-3), 4.24 (s, 2H, CH_2), 7.78–7.31 (m, 5H, Ar–H), and 8.66 (s, 1H, NH). Elemental analysis calculated for $C_{15}H_{14}N_4S$: C, 63.80; H, 5.00; N, 19.84. Found: C, 64.12; H, 5.09; N, 20.07.

*2-Amino-4,5,6,7-tetrahydrobenzo[b]thiophene-3-carbonitrile (**2b**)*

Sulfur (127 mg, 3.96 mmol) was added to a solution of cyclohexanone (3.96 mmol) in ethanol (25 ml) and malononitrile (3.96 mmol). The mixture was stirred at 45°C. Morpholine (5.54 mmol) was added dropwise over 15 min. The mixture was further stirred at 60°C for 18 hr. The mixture was filtered while hot and the resulting crystals were washed with 30% ethanol and dried.[28] Melting point: 138–140°C (yield: 80%) as reported.[29] Mass spectrum: *m/z* (%) 180 (M^++2), 179, 178, 151, and 150.

*4-Chlorocyclohexa[4:5]thieno[2,3-d]-1,2,3-triazine (**3b**)*

A solution of sodium nitrite (1 gm, 16 mmol) was added to a mixture of compound **2b** (10 mmol), HCl (10 ml, 5%), and glacial acetic acid (10 ml). The mixture was stirred at 0–5°C for 1 hr, then for 2 hr at 20°C. The mixture was poured into 100 ml of water and the precipitate was separated by filtration, washed with water, and dried.[19] Melting point: 116–118°C (yield: 81.8%) as reported.[30] Mass spectrum: *m/z* (%): 227 (M^++2), 225, 211, 195, 192, and 150.

4.1.3 | General procedure for the synthesis of compounds 4c,d, 5c,d, 6b, and 7b

A mixture of equimolar amounts (0.01 mol) of compound **3b** and (0.01 mol) of aromatic amines in dry pyridine (10 ml) was refluxed for 16 hr. The mixture was filtered while hot and washed with ice-water. The precipitate was then recrystallized from ethanol.[22]

*N-(5,6,7,8-Tetrahydro-7H-cyclohexa[4:5]thieno[2,3-d]-1,2,3-triazin-4-ylamino)pyrazolo[3,4-b]pyridin-3-amine (**4c**)*

Melting point: 128–130°C (yield: 65%). Mass spectrum: *m/z* (%): 325 (M^++2), 324, 323, 312, 311, 280, and 206. IR (cm^{-1}): 817 (C–S), 1,519 (C=N), and 3,325 (N–H). ^{1}H-NMR (DMSO-d_6, 400 MHz): δ (ppm) = 1.63–1.46 (m, 4H, H-2, H-3), 2.16 (t, J = 7.1 Hz, 2H, H-1), 2.67 (t, J = 7.1 Hz, 2H, H-4), 6.93 (s, 1H, H-5), 7.48–7.18 (m, 3H, Ar–H), and 8.91 (s, 1H, H-6). Elemental analysis calculated for $C_{15}H_{13}N_7S$: C, 55.71; H, 4.05; N, 30.32. Found C, 55.64; H, 4.19; N, 30.71.

*N-(5,6,7,8-Tetrahydro-7H-cyclohexa[4:5]thieno[2,3-d]-1,2,3-triazin-4-ylamino)4,6-dimethylpyrazolo[3,4-b]pyridin-3-amine (**4d**)*

Melting point: 128–130°C (yield: 68%). Mass spectrum: *m/z* (%): 351 (M^+), 350, 346, 332, 267, and 123. IR (cm^{-1}): 767 (C–S), 1,593 (C=N), and 3,294 (NH). ^{1}H-NMR (DMSO-d_6, 400 MHz): δ (ppm) = 1.38–1.15 (m, 4H, H-2, H-3), 1.51 (t, J = 7.1 Hz, 2H, H-1), 1.53 (t, J = 7.1 Hz, 2H, H-4), 3.65 (s, 3H, CH_3), 3.68 (s, 3H, CH_3), 7.44 (s, 1H, Ar–H), 9.89 (s, 1H, H-5), and 10.20 (s, 1H, H-6). Elemental analysis calculated for $C_{17}H_{17}N_7S$: C, 68.10; H, 4.88; N, 27.90. Found: C, 68.37; H, 4.93; N, 28.21.

*N-(5,6,7,8-Tetrahydro-7H-cyclohexa[4:5]thieno[2,3-d]-1,2,3-triazin-4-ylamino)oxazolo[3,4-b]pyridin-3-amine (**5c**)*

Melting point: 200°C (yield: 60%). Mass spectrum: *m/z* (%): 325 (M^++1), 324, 280, 255, 212, 206, and 150. IR (cm^{-1}): 771 (C–S), 1,384 (C–O), 1,627 (C=N), and 3,421 (N–H). ^{1}H-NMR (DMSO-d_6, 400 MHz): δ (ppm) = 1.37–1.15 (m, 4H, H-2, H-3), 2.51 (t, J = 7.1 Hz, 2H, H-1), 2.71 (t, J = 7.1 Hz, 2H, H-4), 7.61–7.30 (m, 3H, Ar–H), and 11.83 (s, 1H, NH). Elemental analysis calculated for $C_{15}H_{12}N_6OS$: C, 55.54; H, 3.73; N, 25.91. Found C, 55.82; H, 3.35; N, 25.64.

*N-(5,6,7,8-Tetrahydro-7H-cyclohexa[4:5]thieno[2,3-d]-1,2,3-triazin-4-ylamino)-4,6-dimethyloxazolo[3,4-b]pyridin-3-amine (**5d**)*

Melting point: 198–200°C (yield: 64%). Mass spectrum: *m/z* (%): 354 (M^++2), 352, 351, 334, 251, and 107. IR (cm^{-1}): 759 (C–S), 1,384 (C–O), 1,624 (C=N), and 3,352 (N–H). ^{1}H-NMR (DMSO-d_6, 400 MHz): δ (ppm) = 1.56–1.18 (m, 4H, H-2, H-3), 1.51 (t, J = 7.1 Hz, 2H, H-1), 2.14 (t, J = 7.1 Hz, 2H, H-4), 2.57 (s, 3H, CH_3), 2.60 (s, 3H, CH_3), 6.87 (s, 1H, Ar–H), and 8.91 (s, 1H, NH). Elemental analysis calculated for $C_{17}H_{16}N_6OS$: C, 57.94; H, 4.58; N, 23.85. Found C, 57.49; H, 4.26; N, 23.52.

*3-(5,6,7,8-Tetrahydro-7H-cyclohexa[4:5]thieno[2,3-d]-1,2,3-triazin-4-ylamino)benzene-1,3-diamine (**6b**)*

Melting point: 128–130°C (yield: 65%). Mass spectrum: *m/z* (%): 297 (M^+), 255, 236, 147, 95, and 43. IR (cm^{-1}): 771 (C–S), 3,197 (N–H), and 3,309 (NH_2). ^{1}H-NMR (DMSO-d_6, 400 MHz): δ (ppm) = 1.6–1.20 (m, 4H, H-2, H-3), 1.76 (t, J = 7.1 Hz, 2H, H-1), 2.57 (t, J = 7.1 Hz, 2H, H-4), 5.49 (s, 2H, NH_2), 7.25–6.95 (m, 3H, Ar–H), 8.10 (s, 1H, ArH-5), and 11.88 (s, 1H, NH). ^{13}C-NMR (DMSO-d_6, 100 MHz): δ (ppm) = 24.6 (C-1), 23.9 (C-2, C-3), 23.8 (C-4), 127.8 (C-5), 142.7 (C-6), 153.3 (C-7), 115.9 (C-8), 93.2 (C-10), 114.6 (C-11), 131.2 (C-12), 104.6 (C-13), 142.7 (C-14), and 146.7 (C-15). Elemental analysis calculated for $C_{15}H_{15}N_5S$: C, 60.58; H, 5.08; N, 23.55. Found C, 60.27; H, 5.36; N, 23.21.

*3-(5,6-Dihydro-7H-cyclohexa[4:5]thieno[2,3-d]-1,2,3-triazin-4-ylamino)benzylamine (**7b**)*

Melting point: 124–126°C (yield: 60%). Mass, spectrum: *m/z* (%): 297 (M^++1), 296, 268, 240, 212, and 91. IR (cm^{-1}): 694 (C–S), 1,573 (C=N), and 3,313 (NH). ^{1}H-NMR (DMSO-d_6, 400 MHz): δ (ppm) = 2.21–1.79 (m, 4H, H-2, H-3), 2.23 (t, J = 7.1 Hz, 2H, H-4), 3.17 (t, J = 7.1 Hz, 2H, H-1), 3.86 (s, 2H, CH_2), 7.09 (m, 5H, Ar–H), and

9.87 (s, 1H, NH). Elemental analysis calculated for $C_{16}H_{16}N_4S$: C, 64.84; H, 5.44; N, 18.90 Found: C, 65.12; H, 5.52; N, 19.14.

4.2 | Biological assays

4.2.1 | Cytotoxic activity against H1299

Potential cytotoxicity of the compounds was tested using Skehan method (Supporting Information).[24]

4.2.2 | Measurement of human EGFR in H1299 cell culture

The measurement of human EGFR in H1299 cell culture was performed by using human EGFR ELISA kit as reported (Supporting Information).[31,32]

4.2.3 | Measurement of potential EGFR inhibitory activity IC_{50}

The measurement of potential EGFR inhibitory activity IC_{50} was performed using Kinase-Glo Plus luminescence kinase assay kit (#V3772; Promega; Supporting Information).[33]

4.3 | Molecular modeling study

In the current research, a molecular modeling study was conducted using the Glide docking function incorporated in the Schrodinger-10.1 molecular modeling program. The X-ray crystal structure of the catalytic domain of the EGFR enzyme in complex with erlotinib (PDB ID: 1M17 resolution 2.6 Å) was obtained from Protein Data Bank (PDB; http://www.rcsb.org/pdb). The EGFR–erlotinib complex was refined for the Glide docking calculations using the protein preparation wizard applying the OPLS-2005 force field. In the second step, water of crystallography, if present, was removed and the pH was adjusted to 7.0. In the third step, the appropriate charge and protonation state of protein were adjusted by the protein assignment script, and then the protein–inhibitor complex was subjected to energy minimization until the (RMSD) value of the nonhydrogen atoms reached 0.3 Å to discard the steric clashes.[34–36]

Using ligand preparation wizard, the 3D structures of the thieno[2,3-*d*][1,2,3]triazine derivatives were constructed and optimized with the build-panel in Maestro. Partial atomic charges were ascribed for the thieno[2,3-*d*][1,2,3]triazine derivatives using the OPLS-2005 force field and possible ionization states were generated at pH 7. To soften the potential for nonpolar parts of the receptor, the van der Waals radii of receptor atoms were scaled by 0.8 with a partial atomic charge of 0.15. A grid box with coordinates $X = 10$, $Y = 10$, and $Z = 10$ was generated at the centroid of the active site. Furthermore, the energy of the obtained ligand structures was minimized until it reached the RMSD cutoff of 0.01 Å. After adjusting the EGFR receptor and the thieno[2,3-*d*][1,2,3]triazine molecules in the correct form, the properties of the active site of EGFR were characterized using "grid generation panel" in Glide.[34–36]

In the final step, the thieno[2,3-*d*][1,2,3]triazine derivatives were docked within the active site of EGFR using the optimized protein–ligand geometries. The extra precision Glide scoring function is applied to rank the docking poses and to assess the protein–ligand binding affinities. Maestro's Pose Viewer utility was utilized to visualize and analyze the key elements of ligand–receptor interaction. The final best-docked structure with the lowest energy was chosen using a Glide score function and selected for further experiments. Erlotinib was removed from the crystal structure EGFR receptor and then redocked using the previously mentioned step to evaluate the accuracy and precision of the established docking protocol.[34–36]

4.4 | Computational calculation

All calculations were performed using the DFT method and the Gaussian 09 program package. With the standard basis set, 6-311++G (d,p) levels of the theory was used for geometry optimizations.[37]

4.5 | Lipinski's rule for drug likeliness and in silico ADME prediction

Drug-likeness properties of the newly synthesized compounds, with expected biological and/or pharmacological activity, were evaluated according to Lipinski's rule of five, which was utilized to determine whether these compounds have the properties that would allow them to be a likely orally active drug in humans. Lipinski's rule of five prescribes ADME, which is absorption, distribution, metabolism, and excretion. The drug-like behavior of our compounds was predicted by using QikProp module (v4.2; Schrodinger 2015-1). The thieno[2,3-*d*][1,2,3]triazine compounds prepared by LigPrep module (v3.1; Schrodinger 2015-1) in the previous step were applied for the calculation of pharmacokinetic parameters by QikProp v4.2.[38]

4.6 | QSAR

4.6.1 | Data set

A set comprising 18 compounds bearing tetrahydrobenzothieno[2,3-*d*]-[1,2,3]triazine and dihydrocyclopentathieno[2,3-*d*][1,2,3]triazine scaffolds were synthesized and selected to establish the QSAR model. The inhibition potencies of the target compounds involved in data set were reported as IC_{50} values varied from 25 to 58 nM. The IC_{50} values were converted into molar values, which were then converted into pIC_{50} values using the following formula:

$$pIC_{50} = -\mathrm{Log}\,(IC_{50}).$$

The 3D structures of thienotriazine derivatives were created using the builder panel in Maestro. Furthermore, these structures were optimized using LigPrep module (v2.1; Schrodinger 2015-1) as described above.

4.6.2 | Pharmacophore 3D-QSAR modeling

Phase (v4.1; Schrodinger 2015-1) was utilized to generate pharmacophore and 3D-QSAR models for EGFR inhibitors. The prepared ligands with their respective biological activity values, pIC_{50}, were imported for developing the pharmacophore model of phase. The ligands were ascribed as active with a threshold of $pIC_{50} > 7.0$ and inactive with a threshold of $pIC_{50} < 6.0$. The remaining compounds were regarded as moderately active. In the present study, phase (v4.0) shape screening for flexible alignment of the selected EGFR inhibitors was utilized. The highest active compound **6b** was taken as the template. One hundred conformers were generated with a maximum of 10 conformations per rotatable bonds using the established default. The most important and difficult step is the selection of training and test sets. To establish the QSAR model robustness, a widely utilized approach and a random division was applied. In this method, three trials were run.[39] Pharmacophore sites for thienotriazine training and test included default set of chemical features of phase: one hydrogen bond acceptor (A), one hydrogen donor (D), hydrophobic interaction (H), and two aromatic rings (R).

4.6.3 | Model validation

The QSAR model ADHRR.26 with six components PLS factor was characterized as the best model. The predicted inhibition of EGFR activity of training set ligands provoked a correlation (*R*) of 0.85 with the observed inhibition. The efficacy of model ADHRR.26 was also tested with external validation. Graph of actual value versus predicted value was also plotted.

CONFLICT OF INTERESTS

The authors declare that there is no conflict of interests.

AUTHOR CONTRIBUTIONS

The manuscript was written through the contributions of all authors. All authors have given approval to the final version of the manuscript.

ORCID

Mohamed M. Said http://orcid.org/0000-0001-6997-7870

REFERENCES

[1] M.-H. Jang, M.-C. Shin, S. Lim, S.-M. Han, H.-J. Park, I. Shin, J.-S. Lee, K.-A. Kim, E.-H. Kim, C.-J. Kim, *J. Pharmacol. Sci.* **2003**, *91*, 95.
[2] M. Sudo, T. M. Chin, S. Mori, N. B. Doan, J. W. Said, M. Akashi, H. P. Koeffler, *Cancer Chemother. Pharmacol.* **2013**, *71*, 1325.
[3] G. Scagliotti, J. von Pawel, S. Novello, R. Ramlau, A. Favaretto, F. Barlesi, W. Akerley, S. Orlov, A. Santoro, D. Spigel, *J. Clin. Oncol.* **2015**, *33*, 2667.
[4] Key statistics for lung cancer. https://www.cancer.org/cancer/non-small-cell-lung-cancer/about/key-statistics.html (accessed: 2017).
[5] D. Cronin-Fenton, T. Dalvi, E. Hedgeman, M. Norgaard, L. Petersen, H. Hansen, J. Fryzek, D. Lawrence, J. Walker, A. Mellemgaard, *J. Thorac. Oncol.* **2017**, *12*, S2085.
[6] B. Jeremic, E. Fidarova, V. Sharma, M. Faheem, A. A. Ameira, C. Nasr Ben Ammar, A. Frobe, F. Lau, S. Brincat, G. Jones, *Radiother. Oncol.* **2015**, *116*, 21.
[7] L. Regales, Y. Gong, R. Shen, E. de Stanchina, I. Vivanco, A. Goel, J. A. Koutcher, M. Spassova, O. Ouerfelli, I. K. Mellinghoff, *J. Clin. Invest.* **2009**, *119*, 3000.
[8] F. Janku, I. Garrido-Laguna, L. B. Petruzelka, D. J. Stewart, R. Kurzrock, *J. Thorac. Oncol.* **2011**, *6*, 1601.
[9] C.-H. Yang, H.-C. Chou, Y.-N. Fu, C.-L. Yeh, H.-W. Cheng, I.-C. Chang, K.-J. Liu, G.-C. Chang, T.-F. Tsai, S.-F. Tsai, *Biochim. Biophys. Acta* **2015**, *1852*, 1540.
[10] W. Han, H. Pan, Y. Chen, J. Sun, Y. Wang, J. Li, W. Ge, L. Feng, X. Lin, X. Wang, *PLOS One* **2011**, *6*, e18691.
[11] M. Tiseo, M. Loprevite, A. Ardizzoni, *Curr. Med. Chem.: Anti-Cancer Agents* **2004**, *4*, 139.
[12] A. Antonello, A. Tarozzi, F. Morroni, A. Cavalli, M. Rosini, P. Hrelia, M. L. Bolognesi, C. Melchiorre, *J. Med. Chem.* **2006**, *49*, 6642.
[13] C. Gan, L. Liu, J. Cui, Z. Liu, *Future Med. Chem.* **2017**, *13*, 375.
[14] K. E. Lackey, *Designing Multi-Target Drugs*, Royal Society of Chemistry, **2012**, pp. 181–205.
[15] C.-H. Wu, M. S. Coumar, C.-Y. Chu, W.-H. Lin, Y.-R. Chen, C.-T. Chen, H.-Y. Shiao, S. Rafi, S.-Y. Wang, H. Hsu, *J. Med. Chem.* **2010**, *53*, 7316.
[16] Y. M. Abdel Aziz, M. M. Said, H. A. El Shihawy, K. A. M. Abouzid, *Bioorg. Chem.* **2015**, *60*, 1.
[17] Y. M. A. Aziz, M. M. Said, H. A. El Shihawy, M. F. Tolba, K. A. M. Abouzid, *Chem. Pharm. Bull.* **2015**, *63*, 1015.
[18] S. Bugge, S. J. Kaspersen, S. Larsen, U. Nonstad, G. Bjørkøy, E. Sundby, B. H. Hoff, *Eur. J. Med. Chem.* **2014**, *75*, 354.
[19] M. Said, H. Elshihawy, *Pak. J. Pharm. Sci.* **2014**, 27.
[20] S. Mowafy, A. Galanis, Z. M. Doctor, R. M. Paranal, D. S. Lasheen, N. A. Farag, P. A. Jänne, K. A. M. Abouzid, *Bioorg. Med. Chem.* **2016**, *24*, 3501.
[21] H. Li, S. Zhou, X. Li, D. Wang, Y. Wang, C. Zhou, G. Schmid-Bindert, *Cancer Biother. Radiopharm.* **2013**, *28*, 115.
[22] A. M. Al-Obaid, S. G. Abdel-Hamide, H. A. El-Kashef, A. A. M. Abdel-Aziz, A. S. El-Azab, H. A. Al-Khamees, H. I. El-Subbagh, *Eur. J. Med. Chem.* **2009**, *44*, 2379.
[23] F. A. Yassin, *Chem. Heterocycl. Compd.* **2009**, *45*, 35.
[24] P. Skehan, R. Storeng, D. Scudiero, A. Monks, J. McMahon, D. Vistica, J. T. Warren, H. Bokesch, S. Kenney, M. R. Boyd, *J. Natl. Cancer Inst.* **1990**, *82*, 1107.
[25] H. N. Kang, S.-H. Kim, M. R. Yun, H. R. Kim, S. M. Lim, M.-S. Kim, K.-W. Hong, S.-M. Kim, H. Kim, K.-H. Pyo, *Lung Cancer* **2016**, *95*, 57.
[26] N. Ghareb, M. M. Abdel Daim, N. M. El-Sayed, M. S. Elgawish, *Bioorg. Chem.* **2017**, *71*, 110.
[27] S. Mowafy, N. A. Farag, K. A. M. Abouzid, *Eur. J. Med. Chem.* **2013**, *61*, 132.
[28] K. Gewald, *Chem. Ber.* **1965**, *98*, 3571.
[29] M. G. Assy, M. H. Sherif, A. E. G. E. Amr, O. I. Abdelsalam, M. A. Al-Omar, M. M. Abdalla, I. Ragab, *J. Heterocycl. Chem.* **2013**, *50*, 766.

[30] G. L. Viswanatha, B. J. Priyadarshini, N. Krishnadas, S. Janardhanan, S. Rangappa, S. Hanumanthappa, *Saudi Pharm. J.* **2012**, *20*, 45.
[31] C. T. Kuan, C. J. Wikstrand, D. D. Bigner, *Endocr.-Relat. Cancer* **2001**, *8*, 83.
[32] R. S. Herbst, *Inter. J. Radiat. Oncol. Biol. Phys.* **2004**, *59*, S21.
[33] http://www.bpsbioscience.com/biochemical-based-assays (accessed: 2019).
[34] T. A. Halgren, R. B. Murphy, R. A. Friesner, H. S. Beard, L. L. Frye, W. T. Pollard, J. L. Banks, *J. Med. Chem.* **2004**, *47*, 1750.
[35] R. A. Friesner, J. L. Banks, R. B. Murphy, T. A. Halgren, J. J. Klicic, D. T. Mainz, M. P. Repasky, E. H. Knoll, M. Shelley, J. K. Perry, *J. Med. Chem.* **2004**, *47*, 1739.
[36] R. Abdelhameed, M. S. Elgawish, A. Mira, A. K. Ibrahim, S. A. Ahmed, K. Shimizu, K. Yamada, *RSC Adv.* **2016**, *6*, 20422.
[37] S. H. Ou, R. Soo, *Drug Des. Dev. Ther.* **2015**, *9*, 5641.
[38] J. K. Rho, Y. J. Choi, B.-Y. Ryoo, I. I. Na, S. H. Yang, C. H. Kim, J. C. Lee, *Cancer Res.* **2007**, *67*, 1163.
[39] P. Verma, A. Singh, D. N. Nthenge-Ngumbau, U. Rajamma, S. Sinha, K. Mukhopadhyay, K. P. Mohanakumar, M. Shaquiquzzaman, *Arabian J. Chem.* **2016**, *6*, 153. https://doi.org/10.1016/j.arabjc.2016.09.019

SUPPORTING INFORMATION

Additional supporting information may be found online in the Supporting Information section.

How to cite this article: Elrayess R, Abdel Aziz YM, Elgawish MS, Elewa M, Elshihawy HA, Said MM. Pharmacophore modeling, 3D-QSAR, synthesis, and anti-lung cancer evaluation of novel thieno[2,3-*d*][1,2,3]triazines targeting EGFR. *Arch Pharm Chem Life Sci*. 2020;e1900108. https://doi.org/10.1002/ardp.201900108